ACS APPLIED MATERIALS & INTERFACES

Research Article

www.acsami.org

Photoresponsive Carbohydrate-based Giant Surfactants: Automatic Vertical Alignment of Nematic Liquid Crystal for the Remote-Controllable Optical Device

Dae-Yoon Kim, Sang-A Lee, Dong-Gue Kang, Minwook Park, Yu-Jin Choi, and Kwang-Un Jeong*

Polymer Materials Fusion Research Center & Department of Polymer-Nano Science and Technology, Chonbuk National University, Jeonju, Jeonbuk 561-756, Korea

Supporting Information

ABSTRACT: Photoresponsive carbohydrate-based giant surfactants (abbreviated as $CELA_nD$-OH) were specifically designed and synthesized for the automatic vertical alignment (VA) layer of nematic (N) liquid crystal (LC), which can be applied for the fabrication of remote-controllable optical devices. Without the conventional polymer-based LC alignment process, a perfect VA layer was automatically constructed by directly adding the 0.1 wt % $CELA_1D$-OH in the N-LC media. The programmed $CELA_1D$-OH giant surfactants in the N-LC media gradually diffused onto the substrates of LC cell and self-assembled to the expanded monolayer structure, which can provide enough empty spaces for N-LC molecules to crawl into the empty zones for the construction of VA layer. On the other hand, the $CELA_3D$-OH giant surfactants forming the condensed monolayer structure on the substrates exhibited a planar alignment (PA) rather than a VA. Upon tuning the wavelength of light, the N-LC alignments were reversibly switched between VA and PA in the remote-controllable LC optical devices. Based on the experimental results, it was realized that understanding the interactions between N-LC molecules and amphiphilic giant surfactants is critical to design the suitable materials for the automatic LC alignment.

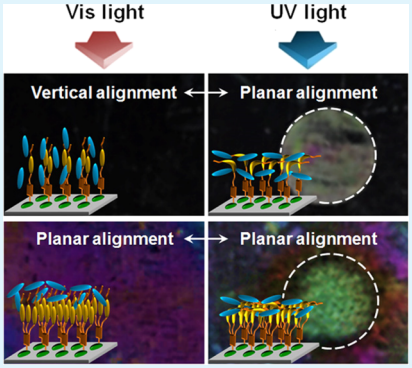

KEYWORDS: *click-chemistry, photochemistry, giant surfactant, amphiphile, liquid crystal alignment*

INTRODUCTION

The control of liquid crystal (LC) alignment is one of the most important technologies for high-performance LC devices such as light shutters, sensors and modulators.[1−8] In LC display (LCD) industries, the molecular orientation of active LC soft materials has been mainly achieved by rubbing the polymer-based alignment film. Among various polymers, the thermally and mechanically stable polyimides exhibiting strong anchoring interactions with the LC molecules have been widely used.[9−15] However, the mechanical contact methods can generate critical drawbacks, such as unstable electric charges, residual stresses and dust particles, which can deteriorate the electrical and optical performances of LCD devices.[16−21] Recently, contact free alignment methods have been intensively investigated to overcome these disadvantages of conventional rubbing methods as well as to cut the manufacturing cost.[22−25]

An alternative method to achieve LC orientation is photoalignment using photochromic materials, such as azobenzene mesogens, cinnamoyl chromophores, spyropyran−merocyanine isomers and coumarine derivatives.[26−30] The nematic (N) LC soft materials have the molecular orientational long-range order only in one dimension (1D), and their macroscopic molecular orientations are effectively controlled by external forces, such as electric and magnetic fields with and without the support of surface alignments.[31−33] Because the molecular conformations of photochromic doping materials can be effectively switched by light, the overall molecular orientations of N-LC can be reversibly controlled. The photomodulation of LC alignment has some advantages due to the contact free and remote-controllable characteristics. Additionally, it can be useful for patterning processes on the flexible substrates, which is an important requirement for the flexible displays and devices.[34−41] Among photochromic materials, the azobenzene derivatives can be promising alignment materials for the LC photomodulating devices because the cooperative conformational changes of azobenzene are reversibly and effectively tuned with respect to the wavelength of light.[42−47]

More recently, the self-assembled materials on the solid surface have been newly introduced for the automatic formation of LC anchoring conditions.[48−51] There are several reports for the modifications of the solid surface for LC alignment layers by directly introducing carbon-based nanomaterials, gold nanoparticles and silane compounds in the N-LC media.[52−57] Among them, amphiphilic supramolecules that consist of hydrophobic tails and hydrophilic head groups are

Received: January 12, 2015
Accepted: March 4, 2015
Published: March 4, 2015

DOI: 10.1021/acsami.5b00259
ACS Appl. Mater. Interfaces 2015, 7, 6195−6204

Scheme 1. Synthesis of $CELA_1D$-OH and $CELA_3D$-OH by a Click Reaction[a]

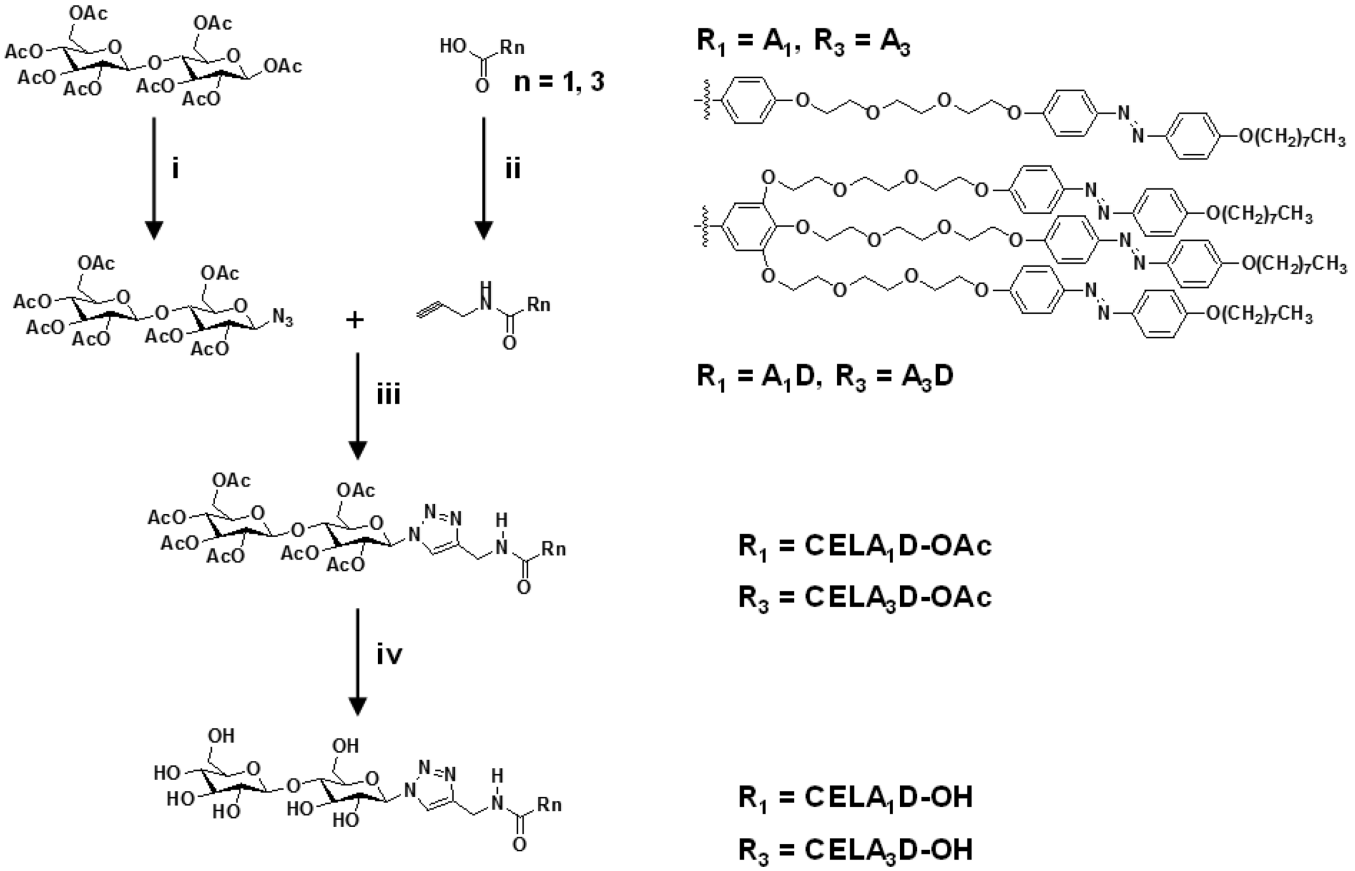

[a]Reagents and conditions: (i) Me_3SiN_3, $SnCl_4$, CH_2Cl_2, 25 °C for 24 h; (ii) EDC, DMAP, CH_2Cl_2, 25 °C for 12 h; (iii) CuBr, PMDETA, DMF, 25 °C for 24 h; (iv) NaOMe, MeOH, amberlyst IR 120, CH_2Cl_2, 25 °C for 12 h.

fairly effective for the fabrication of automatic LC alignment layers.[58] Because the interaction of polar head groups with substrates is usually higher than with hydrophobic N-LC molecules, the initially introduced amphiphiles are phase-separated from the N-LC media and diffused onto the substrates. However, for the fabrication of uniform LC alignment layer, several parameters, such as the initial solubility in N-LC media, the concentration of amphiphiles, the kinetics of phase-separation from the N-LC media and the self-assembly of amphiphilic molecule on the substrates, should be finely controlled.[59]

In this circumstance, we newly designed and synthesized the giant surfactants containing both carbohydrate and azobenzene groups (abbreviated as $CELA_n$-OH, where n = 1 and 3) for the automatic vertical alignment (VA) layer of N-LC, which can be applied for the fabrication of remote-controllable optical devices. The cellobiosyl polar head group is specifically programmed at the end of $CELA_n$-OH amphiphiles to induce the automatic 2D surfactant monolayer on the surface of solid substrates. The VA of N-LC medium was evaluated with respect to the concentration of $CELA_n$-OH surfactants and the number (n) of azobenzene mesogens in $CELA_n$-OH surfactants. The $CELA_1D$-OH giant surfactant in the N-LC medium gradually diffused onto the substrate of LC cell and self-assembled to the expanded monolayer structure, which can construct the VA layer without forming the macroscopic aggregations. On the other hand, the $CELA_3D$-OH compound forming the condensed monolayer structure exhibited a planar alignment (PA) rather than a VA. The reversible VA (LC director is parallel to the surface normal) and PA (LC director is perpendicular to the surface normal) LC orientation was successfully demonstrated by tuning the wavelength of light, which can allow us to fabricate the remote-controllable and photopatternable LC optical devices.

RESULT AND DISCUSSION

Programmed Photochromic Carbohydrate-based Giant Surfactants. A series of carbohydrate-based giant surfactants is newly designed and synthesized for the automatic VA layer of N-LC, which can be applied for the fabrication of remote-controllable optical devices. Utilizing the copper(I)-catalyzed azide−alkyne [3 + 2] cycloaddition reaction, the azobenzene-based dendritic alkyne derivatives are click-coupled with a cellobiosyl azide compound.[60−62] Depending on the number (n) of azobenzene mesogens, the photoresponsive carbohydrate-based giant surfactants are abbreviated as $CELA_nD$-OH. As shown in Scheme 1, the azobenzene mesogenic group with a hydrocarbon tail is specifically chosen to enhance the interactions with N-LC medium and to modulate the alignment of N-LC medium by irradiating light. The nanophase separation within the giant surfactants and against the N-LC medium can be finely tuned by introducing hydrophilic triethyleneoxide connectors and hydrophobic alkyl chains. The nondendritic azobenzene acid $\mathbf{A_1}$ and dendritic azobenzene acid $\mathbf{A_3}$ are first prepared by the functionalization with methyl paraben and methyl gallate, respectively.[38] According to

DOI: 10.1021/acsami.5b00259
ACS Appl. Mater. Interfaces 2015, 7, 6195−6204

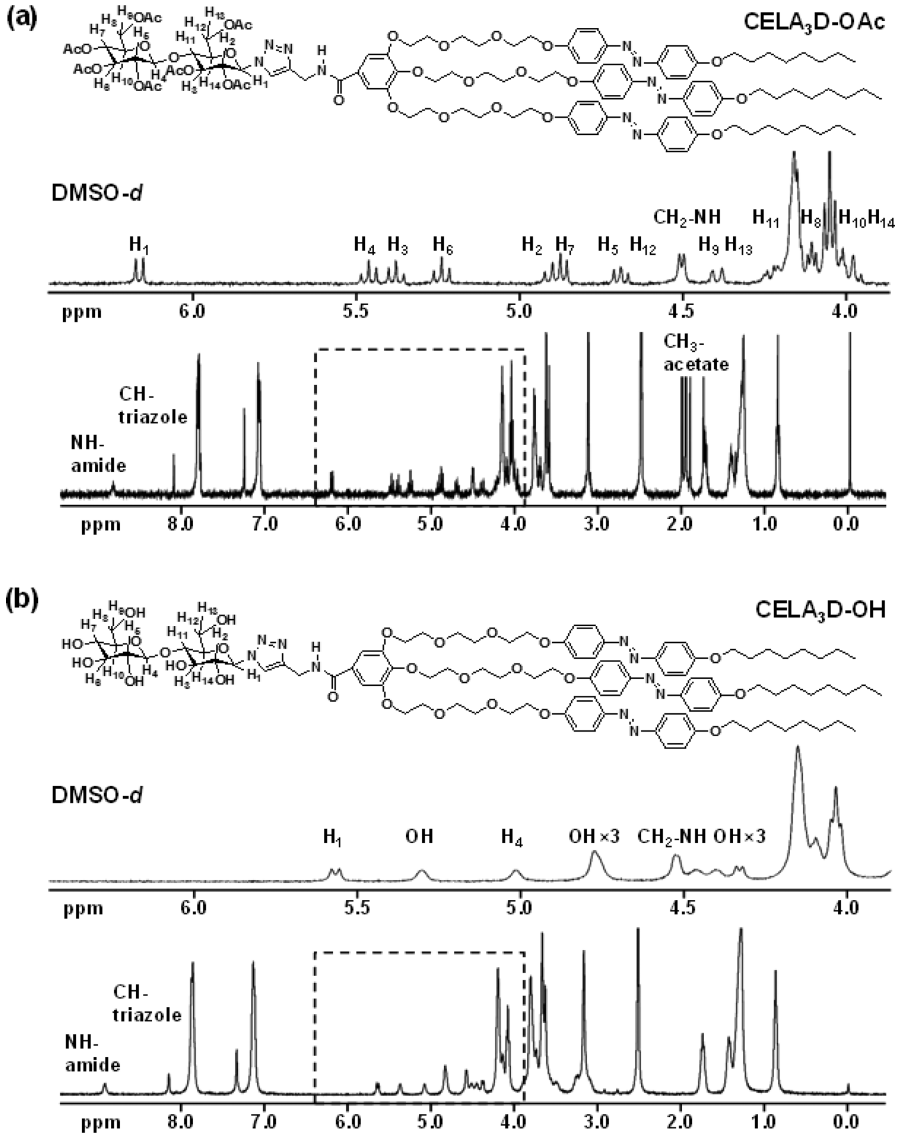

Figure 1. ^{1}H NMR spectra of CELA$_3$D-OAc (a) and CELA$_3$D-OH (b) in deuterated dimethyl sulfoxide solution at 25 °C.

the reference reported by Paulsen, the cellobiosyl azide is synthesized in a stereoselective manner by treating acetylated cellobiosyl compound with trimethylsilyl azide and tin tetrachloride (Scheme 1).[63] This compound can react via the 1,3-dipolar cycloaddition with propargyl amides of the azobenzene acids. To introduce the alkyne, the propargyl amide derivatives **A$_1$D**, and **A$_3$D** are synthesized in the presence of EDC and DMAP coupling reagents, as shown in Scheme 1. The click reaction is conducted in the anhydrous condition using CuBr and PMDETA to obtain the desired products. All of the acetyl protected derivatives are deacetylated at room temperature to obtain the giant surfactants, CELA$_n$D-OH.

As shown in Figure 1, the acetyl protected carbohydrate derivative (CELA$_3$D-OAc) and its deacetylated carbohydrate derivative (CELA$_3$D-OH) are fully characterized by proton (^{1}H) nuclear magnetic resonance (NMR) spectroscopy. By deacetylating the cellobiosyl octa-acetate carbohydrate group of CELA$_3$D-OAc (Figure 1a) with MeONa and Amberlyst IR120, the protons of acetyl groups are completely disappeared around 2.0 ppm, and the seven alcohol peaks of deacetylated cellobiosyl carbohydrate group of CELA$_3$D-OH are newly developed, as represented in Figure 1b. Additionally, it is identified that the protons at deacetylated cellobiosyl carbohydrate group (from H_1 to H_{14}) in the CELA$_3$D-OH are shifted to the upfield because the adjacent electron-withdrawing acetyl groups in the CELA$_3$D-OH are removed. The detailed synthetic procedures are explained in the Experimental Section. Chemical structures and purities of CELA$_n$D-OH and their intermediates are confirmed by thin layer chromatography (TLC), ^{1}H NMR (see Figures S1−S6 in the Supporting Information) and matrix-assisted laser desorption/ionization time-of-flight (MALDI-ToF) mass spectrometry (Figures S7 and S8 of the Supporting Information).

Automatic LC Alignment by Carbohydrate-based Giant Surfactants. The self-organization of amphiphilic surfactants on solid surfaces via strong hydrogen bonding is one of the most convenient strategies to develop the photoalignment layer for N-LC molecules. Because the interaction between carbohydrates' polar head groups with substrates is higher than with N-LC molecules, CELA$_n$D-OH molecules tend to act as surfactants between the hydrophobic N-LC medium and the hydrophilic solid substrate. Generally, the amphiphilic surfactants consist of three blocks: the head groups directly interacting with the solid substrate, the linkages

DOI: 10.1021/acsami.5b00259
ACS Appl. Mater. Interfaces 2015, 7, 6195−6204

with specific functions between head and tail groups and the tail groups determining the interaction parameters with N-LC molecules.[58] In the CELA$_n$D-OH giant surfactants, the cellobiosyl carbohydrate moiety is selectively chosen for the polar head group. Because there are seven alcohols in the cellobiosyl carbohydrate group of CELA$_n$D-OH, it is very effective to make phase-separation against the N-LC medium and form the strong hydrogen bondings with the hydrophilic ITO substrates. Therefore, the CELA$_n$D-OH surfactant directly mixed with N-LC hosts at the initial state should be phase-separated against the N-LC media and diffused onto the substrates, which is a thermodynamically more stable state. By introducing the photochromic azobenzene moiety in the CELA$_n$D-OH surfactant, the alignment of the N-LC can be reversibly switched with respect to the wavelength of irradiated light. The newly synthesized CELA$_n$D-OH giant surfactants can be ideal N-LC alignment materials, which can allow us fabricated the remote-controllable and photopatternable LC optical devices.

To realize this proposal, four N-LC/CELA$_n$D-OH mixtures with different contents of CELA$_n$D-OH from 5.0 to 0.1 wt % are first prepared by utilizing a vortex mixer, as tabulated in Figure 2. After the mixtures are stirred for 30 min above the

Nematic liquid crystal: MLC 6873-100 (Merck Co.)

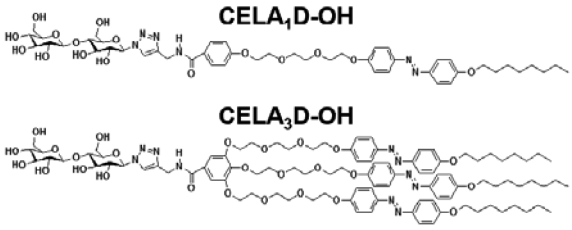

	Composition (wt%)			
CELA$_n$D-OH	5.0	1.0	0.5	0.1
NLC	95.0	99.0	99.5	99.9

Figure 2. Materials information: host nematic liquid crystal (N-LC, MLC 6873-100), photoresponsive giant surfactants (CELA$_n$D-OH) and the N-LC/CELA$_n$D-OH mixtures with different weight ratios.

isotropization temperatures of CELA$_n$D-OH and N-LC constituents, the homogeneously mixed samples are gradually cooled down to ambient temperature. The test LC cells are fabricated by sandwiching the mixtures between two precleaned ITO glass substrates. The cell gap is controlled to be 10 μm by applying spacers. Here, the N-LC/CELA$_n$D-OH mixtures are filled into the LC cells on a 120 °C hot plate utilizing the one drop filling (ODF) process method, which can avoid the flow effect, and are then cooled down to room temperature.[64]

Upon varying the content of CELA$_n$D-OH surfactants in the N-LC/CELA$_n$D-OH mixtures from 5.0 to 0.1 wt %, POM images with transmissive mode are taken (Figure 3). Whether the N-LC host molecules are vertically aligned or not is evaluated at first by the darkness of the transmissive POM image (Figure 3) and second confirmed by the formation of the Maltese cross, viewed under conoscopic microcopy with a Bertrand lens (insets of Figure 3). Note that the vertical

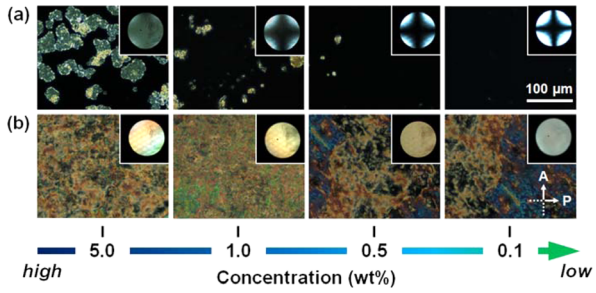

Figure 3. Orthoscopic and conoscopic (inset) POM images of the LC test cells with different weight ratios of N-LC/CELA$_1$D-OH (a) and N-LC/CELA$_3$D-OH (b) mixtures.

orientation of N-LC should exhibit a dark state under cross-polarized POM (polarizer and analyzer are arranged at a right angle with respect to each other) because the long axis of the N-LC molecule is aligned normal to the surface of test LC cells and does not exhibit any birefringence (zero birefringence effect). The formation of a Maltese cross in the conoscopic POM image is direct evidence of the VA of the LC test cell because the dark state of the LC POM image is also observed when the long axis of the N-LC molecule is parallel to the polarizer or the analyzer (zero amplitude effect).[59] The strong birefringence in the wide area of 5.0 wt % CELA$_1$D-OH test cell clearly indicates that there are great amount of macroscopic CELA$_1$D-OH aggregations (Figure 3a). By decreasing the content of CELA$_1$D-OH surfactant in the N-LC/CELA$_1$D-OH mixtures, the dark area gets broader in the transmissive POM image and the Maltese cross in the conoscopic POM image gets more obvious. When the amount of CELA$_1$D-OH surfactant is reduced to 0.1 wt %, any CELA$_1$D-OH aggregates in the N-LC/CELA$_1$D-OH mixture are detected in the macroscopic area, and a perfect VA of N-LC is achieved with a clear Maltese cross in the conoscopic POM image. On the contrary, as shown in Figure 3b, it is apparent that CELA$_3$D-OH surfactant does not induce the VA of N-LC medium, but the PA. Unlike the CELA$_1$D-OH surfactant, the solubility of CELA$_3$D-OH in the N-LC medium is high enough not to make macroscopic aggregations of CELA$_3$D-OH even at the 5.0 wt % CELA$_3$D-OH test cell. It is worth noting that not all the CELA$_1$D-OH surfactants are on the substrates and some of them are still dissolved in the N-LC medium at room temperature, which physical phenomena should be further studied in the future.

When the LC cell with 0.1 wt % CELA$_1$D-OH is slowly cooled down at 2.5 °C/min (a slow cooling) from 120 °C to the room temperature, a perfect dark state without any light leakage is obtained, as shown in Figure 3a. However, if the LC cell with the 0.1 wt % CELA$_1$D-OH is fabricated by cooling the LC cell at 40 °C/min (a fast cooling), several bright spots are detected. This result represents the fact that the CELA$_1$D-OH monolayer can be constructed by not only optimizing the concentration of CELA$_1$D-OH in the LC mixture but also tuning the rates of the phase-separation from the N-LC medium as well as the diffusion of CELA$_1$D-OH onto the substrates. Because the compatibility and interaction of CELA$_n$D-OH with N-LC media are properly tuned by covalently connecting the nondendritic (n = 1) and dendritic (n = 3) azobenzene derivatives, the initially dissolved CELA$_n$D-OH in the N-LC is gradually phase-separated from the N-LC medium and diffused onto the solid surface of the LC test cell and then constructs the CELA$_n$D-OH monolayer film, which is

DOI: 10.1021/acsami.5b00259
ACS Appl. Mater. Interfaces 2015, 7, 6195−6204

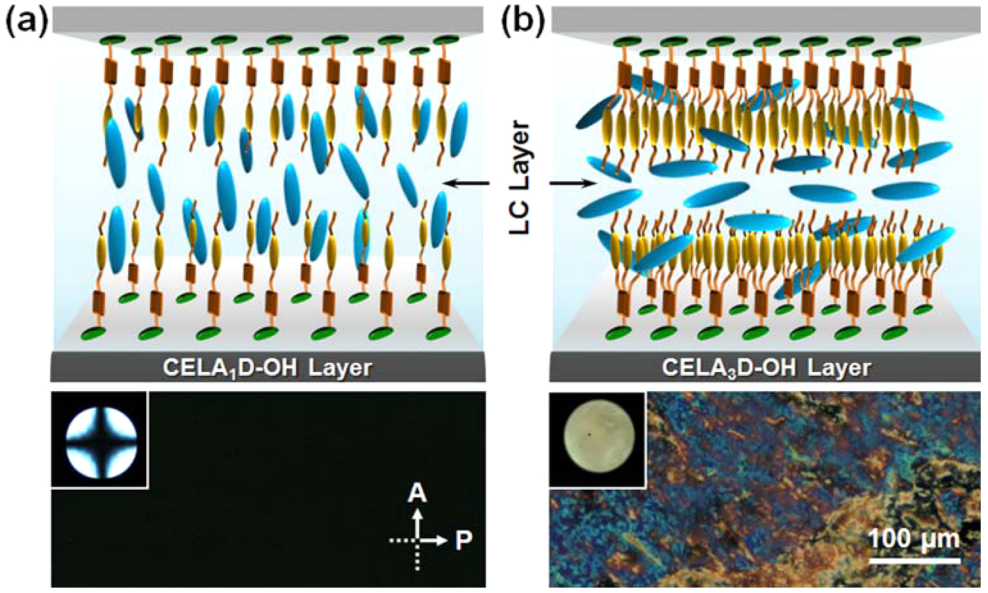

Figure 4. POM images (bottom) and their schematic illustrations (top) of the vertically aligned LC test cells filled with the 0.1 wt % of $CELA_1D$-OH (a) and $CELA_3D$-OH (b) surfactants.

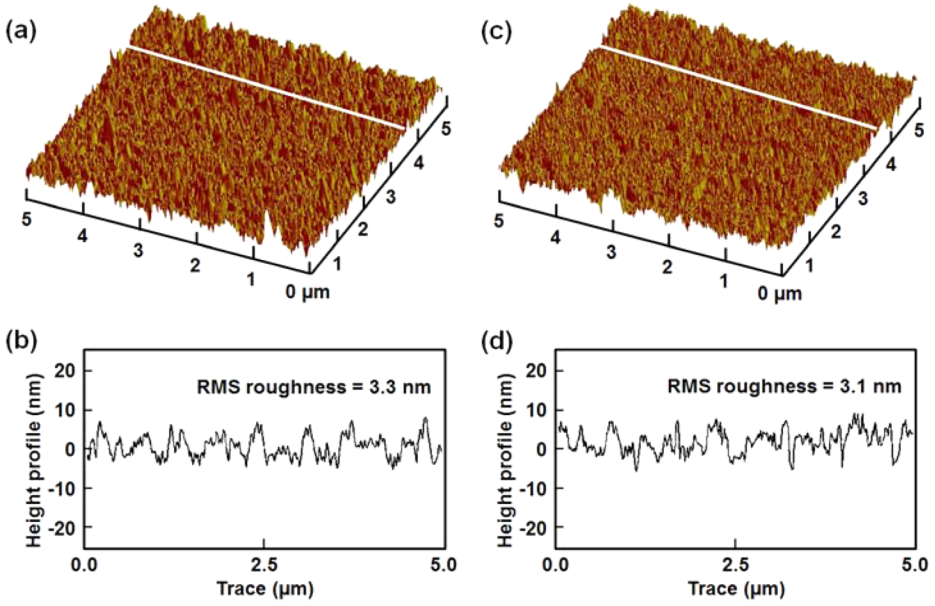

Figure 5. 3D topographic AFM images (a, c) and their corresponding height profiles (b, d) of the 0.1 wt % of $CELA_1D$-OH (a, b) and $CELA_3D$-OH (c, d) monolayer film on the ITO coated glass substrates.

an ideal surface structure for the formation of the alignment layer of N-LC.

Formation of Two-Dimensional Monolayered Surfactant Protrusions. Uniform $CELA_nD$-OH monolayers can be constructed by the phase-separation from N-LC media and the diffusion to the solid surfaces and then the self-assembly on the solid surfaces. The formation of the $CELA_nD$-OH surfactant monolayer is confirmed by a specifically designed experiment. The ITO substrates are first dipped in the 0.1 wt % of $CELA_nD$-OH/THF solution for 1 h, and tetrahydrofuran (THF) solvent on the substrates of the LC cell is slowly evaporated for 12 h. Due to the good solubility of $CELA_nD$-OH surfactants in common organic solvents such as THF, $CELA_nD$-OH surfactants can be easily fabricated into films by a simple dipping method. Note that the predoped ITO substrates with $CELA_nD$-OH are not much changed, even after several mild rinses with THF. This means that the once formed $CELA_nD$-OH monolayers on the ITO glass substrates are strong enough against the chemical attacks because of the hydrogen bonding interactions between the cellobiosyl polar head groups of $CELA_nD$-OH surfactants and the hydrophilic ITO glass substrates. The preformed $CELA_nD$-OH monolayers are carefully warmed to evaporate the solvent for 1 h to ensure complete removal of the residual solvent before filling the N-LC. Identical to the results of Figure 3 (the direct mixing with N-LC host), the VA and PA of N-LC are achieved again by the preformed $CELA_1D$-OH and $CELA_3D$-OH monolayers (Figure 4a,b), respectively.

To investigate the monolayer formation of the $CELA_nD$-OH on the solid surface, the morphological observations of the

DOI: 10.1021/acsami.5b00259
ACS Appl. Mater. Interfaces 2015, 7, 6195−6204

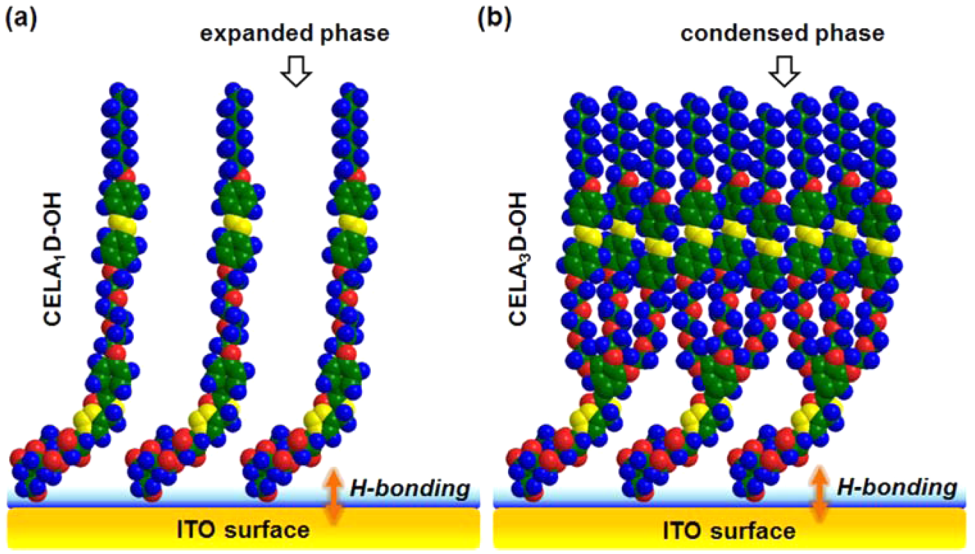

Figure 6. Schematic illustrations for the expanded phase of the $CELA_1D$-OH (a) and the condensed phase of the $CELA_3D$-OH (b) surfactant monolayers on the ITO coated glass substrates.

preformed $CELA_nD$-OH substrates are conducted by atomic force microscopy (AFM). The surface of bare ITO substrate is also studied as a reference, which shows a relatively smooth surface (Figure S9 of the Supporting Information). As shown in Figure 5a, the 0.1 wt % $CELA_1D$-OH coated surface exhibits many protrusions but constructs the uniform continuous layer in each protrusions. The average width and height of protrusions of the $CELA_1D$-OH layers (Figure 5b) are in the range of 167.9 and 4.1 nm, respectively, and the root-mean-square (RMS) surface roughness is about 3.3 nm. The height profile of the 0.1 wt % $CELA_3D$-OH as shown in Figure 5c is almost identical to that of the $CELA_1D$-OH coated surface. The average height of protrusions and RMS surface roughness of $CELA_3D$-OH layers (Figure 5d) are in the range of 4.3 and 3.1 nm, respectively. This result indicates that there is no significant surface topographical difference between $CELA_nD$-OH layers. Because the calculated geometric length of $CELA_nD$-OH along the long axis is about 4.8 nm (Figure S10 of the Supporting Information), it can be understood that the $CELA_nD$-OH surfactants are deposited and laterally self-assembled to the monolayers, in which the molecular long axis of $CELA_nD$-OH is parallel to the surface normal.

The tethered azobenzene mesogens with alkyl chains of $CELA_nD$-OH can make the physical interactions with N-LC molecules near to the substrates and provide enough empty spaces for N-LC molecules to crawl into the empty zones, which results in the creation of vertical LC alignment. However, as shown in Figure 4, it is clear that the orientation of N-LC does not always follow the surface morphology. In the case of the 0.1 wt % $CELA_1D$-OH doped LC test cell, it is well matched with our understanding that the N-LC molecules align along the parallel to the long axis of the vertically oriented $CELA_1D$-OH monolayer. Meanwhile, the $CELA_3D$-OH monolayer induces the PA of N-LC medium even though the molecular long axis of $CELA_3D$-OH is normal to the surface. Therefore, it is realized that the alignment of N-LC is closely related not only to the morphological aspects of protrusion domains but also to the molecular packing structures of $CELA_nD$-OH monolayers. As schematically illustrated in Figure 6a, the $CELA_1D$-OH surfactant can form the expanded structure on the surface so that the N-LC molecules in the medium can partly penetrate into the $CELA_1D$-OH expanded structures for the formation of VA. When the number (n) of azobenzene mesogens in $CELA_nD$-OH surfactants is increased from 1 to 3, the condensed structure is constructed on the surface (Figure 6b). The N-LC molecules cannot crawl into the $CELA_3D$-OH condensed structures but lie down for the formation of PA.[65] Thus, it is concluded that the LC alignment crucially depends on the molecular interactions between the N-LC media and the alignment layers.

Remote-Controllable N-LC Molecular Alignments. The photochemical behaviors of the $CELA_1D$-OH and $CELA_3D$-OH surfactants are investigated by ultraviolet−visible (UV−vis) spectroscopy in a chloroform solution, and the results are summarized in Figure 7. Upon irradiating the UV light with a maximum intensity at 365 nm, the thermodynamically stable *trans*-azobenzene conformer of $CELA_1D$-OH transforms to its metastable cis conformer and reaches into a new photostationary state in 50 s. As indicated in Figure 7a, the absorption band between two isosbestic points (320 and 430 nm) resulting in the π-to-π^* transition is originated from the trans conformer

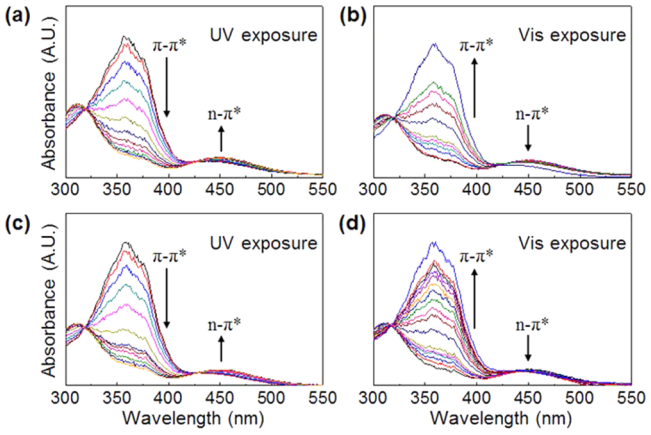

Figure 7. UV−vis absorption spectra of $CELA_1D$-OH (a, b) and $CELA_3D$-OH (c, d) by irradiating the 365 nm (a, c) and 450 nm (b, d) lights, respectively.

DOI: 10.1021/acsami.5b00259
ACS Appl. Mater. Interfaces 2015, 7, 6195−6204

of azobenzene, whereas the ground state (n) of the cis conformer of azobenzene is excited to the π^* state by absorbing the UV light in the range of 430−540 nm. As subsequently exposing the visible light, the amount of trans conformational azobenzene isomer is increased by concomitantly decreasing the intensity and area of the absorption band for the trans/cis isomers of azobenzene in 30 min (Figure 8b). The trans-to-cis

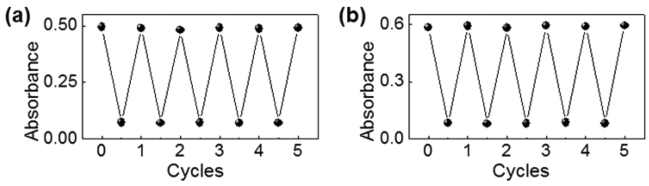

Figure 8. Absorption changes of $CELA_1D$-OH (a) and $CELA_3D$-OH (b) by alternating UV and visible light irradiation.

and cis-to-trans photoisomerization properties are also observed in the case of $CELA_3D$-OH surfactant, as described in Figure 7c,d. The fatigue resistances of $CELA_nD$-OH are examined by the absorption at 365 nm, as the solutions are repeatedly irradiated with the UV and visible light. Both $CELA_1D$-OH and $CELA_3D$-OH surfactants show excellent fatigue resistances, and no degradation is observed (Figure 8a,b, respectively). Transitions between two photostationary equilibrium states are fully reversible processes by alternating the UV and visible lights, which can allow us to fabricate a reversible photomodulating device.

The peculiar trans−cis photoisomerization process of $CELA_nD$-OH may be useful as a photoalignment layer for the remote-controllable optical devices. However, an efficient trans−cis photoisomerization process of $CELA_nD$-OH is required even in the self-assembled monolayer on the surface. Figure 9 shows the photomicrographs of LC test cells with 0.1 wt % $CELA_nD$-OH monolayers. The LC test cells are placed between two Polaroid films, which are at a right angle. By irradiating the $CELA_1D$-OH surfactant doped LC test cell with the 365 nm UV light through a circular photomask, the UV exposed part is selectively transformed from VA to PA on the spot, as shown in Figure 9a,b. When the irradiated UV light is blocked, the PA of N-LC immediately returns back to the VA. This result clearly demonstrates that the molecular alignment of host N-LC can be effectively tuned by the remote-controllable photoalignment $CELA_1D$-OH monolayer. In the case of $CELA_3D$-OH surfactant doped LC test cell (Figure 9c,d), the initial PA is not changed even after exposing the UV light. This means that the metastable *cis*-azobenzene conformers of $CELA_3D$-OH monolayer do not open the enough empty space for N-LC molecules to penetrate into the $CELA_3D$-OH monolayer for the formation of VA.

CONCLUSIONS

A series of programmed photoresponsive giant surfactants ($CELA_n$-OH) containing both photochromic azobenzene moiety and polar carbohydrate head group was specifically designed and synthesized for the construction of an automatic photoalignment layer without following the conventional polymer-based LC alignment process. From the systematic experiments of $CELA_n$-OH in nematic liquid crystal (N-LC) media, it was found that molecular structures of giant surfactants are critical for controlling the LC alignment behaviors. In the LC cell with the 0.1 wt % $CELA_1$-OH, the

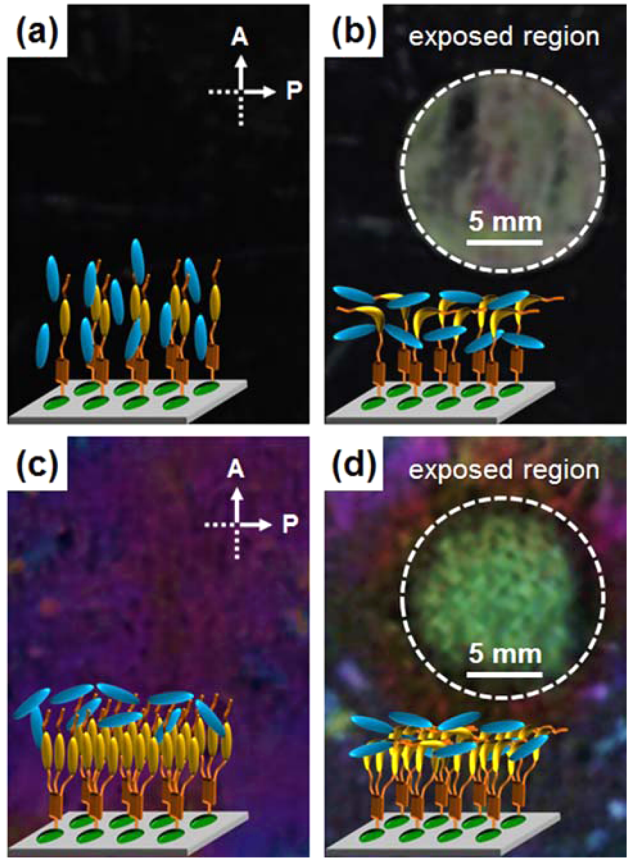

Figure 9. Macroscopic photographs and the corresponding schematic illustrations of the 0.1 wt % $CELA_1D$-OH (a, b) and $CELA_3D$-OH (c, d) LC test cells before (a, c) and after (b, d) UV irradiations with a circular photomask. The LC test cells are placed between two Polaroid films, which are at a right angle.

$CELA_1D$-OH giant surfactants gradually diffused onto the substrates and self-assembled to the expanded monolayer structure, which can provide enough empty spaces for the N-LC molecules to partly penetrate into the expanded structure for the construction of vertical alignment (VA) layer. On the other hand, the $CELA_3D$-OH formed the condensed monolayer structure on the substrates resulting in the planar alignment (PA) rather than the VA, because the N-LC molecules cannot crawl into the condensed structure. Additionally, the photopatternable and remote-controllable characteristics of $CELA_n$-OH doped LC film may provide more opportunities for the addressable displays and optical data storage.

EXPERIMENTAL SECTION

Materials. All reagents were purchased from Aldrich and used without further purification. Solvents were purified before use. Nematic liquid crystal (MLC 6783-100, Merck Co.) was used as received. Cellobiosyl azide[63] and nondendritic and dendritic azobenzene acid compounds[38] were synthesized according to previously described procedures. The detailed synthetic procedures are provided in the Supporting Information.

Synthesis of Compounds A_1D and A_3D. A 100 mL round-bottom flask was charged with nondendritic azobenzene acid compound $\mathbf{A_1}$ (0.30 g, 0.52 mmol), propargyl amine (0.11 g, 2.07 mmol), *N*-(3-(dimethylamino)propyl)-*N*′-ethylcarbodiimide hydrochloride (EDC; 0.39 g, 2.07 mml) and 4-dimethylaminopyridine (DMAP; 0.25 g, 2.07 mmol) in 30 mL of anhydrous CH_2Cl_2. The

DOI: 10.1021/acsami.5b00259
ACS Appl. Mater. Interfaces 2015, 7, 6195−6204

reaction was stirred under a nitrogen atmosphere at room temperature for 12 h. The solvent was removed on a rotary evaporator and the residue was purified by column chromatography on silica gel (THF:CH_2Cl_2 = 1:3) to obtain compound **A_1D** as a yellow solid. The same procedure was followed to prepare compound **A_3D**.

A_1D. Yield: 87% (0.27 g). ^{1}H NMR ($CDCl_3$, 400 MHz): δ = 0.89 (t, 3H), 1.23−1.51 (m, 10H), 1.80 (m, 2H), 2.21 (s, 1H), 3.76 (t, 4H), 3.88 (m, 4H), 4.02 (t, 2H), 4.12 (m, 2H), 4.18 (m, 4H), 6.14 (t, 1H), 6.91 (q, 2H), 6.99 (q, 4H), 7.84 (q, 4H), 7.97 ppm (q, 2H).

A_3D. Yield: 80% (0.25 g). ^{1}H NMR ($CDCl_3$, 400 MHz): δ = 0.89 (t, 9H), 1.23−1.51 (m, 30H), 1.80 (m, 6H), 2.21 (s, 1H), 3.76 (t, 12H), 3.88 (m, 12H), 4.02 (t, 6H), 4.12 (m, 2H), 4.20 (m, 12H), 6.41 (t, 1H), 6.99 (q, 12H), 7.09 (s, 2H), 7.84 ppm (q, 12H).

Synthesis of Compounds $CELA_1D$-OAc and $CELA_3D$-OAc. Propargyl derivative **A_1D** (0.10 g, 0.16 mmol), cellobiosyl azide (0.16 g, 0.24 mmol), copper(I) bromide (0.04 g, 0.24 mmol) and *N*,*N*′,*N*″,*N*″-pentamethyldiethylenetriamine (PMDETA; 0.05 g, 0.24 mmol) were dissolved in anhydrous DMF (10 mL) under nitrogen atmosphere. The mixture was stirred at 25 °C for 24 h. After the catalyst was removed by filtration, the solvent was evaporated under a reduced pressure. Distilled water was added and the product was extracted with $CHCl_3$. The organic phase was dried with $MgSO_4$. After filtration and evaporation, the crude product was purified by column chromatography with silica gel using THF:CH_2Cl_2 = 1:3 to yield $CELA_1D$-OAc as a yellow powder. The same procedure was followed to prepare compound $CELA_3D$-OAc.

$CELA_1D$-OAc. Yield: 85% (0.17 g). ^{1}H NMR (DMSO-*d*, 400 MHz): δ = 0.89 (t, 3H), 1.23−1.54 (m, 10H), 1.80 (m, 2H), 2.01 (m, 21H), 3.65 (t, 4H), 3.77 (m, 4H), 3.92 (s, 1H), 4.01 (s, 1H), 4.08 (t, 2H), 4.11 (t, 1H), 4.18 (m, 4H), 4.25 (s, 1H), 4.38 (s, 1H), 4.43 (s, 1H), 4.51 (d, 2H), 4.71 (s, 1H), 4.75 (d, 1H), 4.85 (d, 1H), 4.89 (d, 1H), 5.24 (t, 1H), 5.37 (t, 1H), 5.45 (t, 1H), 6.24 (d, 1H), 6.99 (d, 2H), 7.02 (q, 4H), 7.78 (q, 4H), 7.81 (d, 2H), 8.09 (s, 1H), 8.78 ppm (s, 1H).

$CELA_3D$-OAc. Yield: 78% (0.11 g). ^{1}H NMR (DMSO-*d*, 400 MHz): δ = 0.89 (t, 9H), 1.23−1.54 (m, 30H), 1.80 (m, 6H), 2.01 (m, 21H), 3.65 (t, 12H), 3.77 (m, 12H), 3.92 (s, 1H), 4.01 (s, 1H), 4.08 (t, 6H), 4.11 (t, 1H), 4.18 (m, 12H), 4.25 (s, 1H), 4.38 (s, 1H), 4.43 (s, 1H), 4.51 (d, 2H), 4.71 (s, 1H), 4.75 (d, 1H), 4.85 (d, 1H), 4.89 (d, 1H), 5.24 (t, 1H), 5.37 (t, 1H), 5.45 (t, 1H), 6.24 (d, 1H), 7.02 (q, 12H), 7.21 (s, 2H), 7.84 (q, 12H), 8.09 (s, 1H), 8.78 ppm (s, 1H).

General Procedure for the Preparation of Compounds $CELA_1D$-OH and $CELA_3D$-OH. The acetyl protected carbohydrate derivative $CELA_1D$-OAc (0.30 g, 0.23 mmol) were fully dissolved in the 10 mL of anhydrous CH_2Cl_2, and anhydrous methanol (10 mL) was additionally added. After sodium methoxide was introduced (0.20 g, 3.52 mmol), the solution was stirred at room temperature for 12 h. After the reaction was finished, amberlyst IR 120 H^+ form was added to exchange the sodium ions, and the resin was filtered off. The crude product was purified by reprecipitation from $CHCl_3$ and methanol, and dried under vacuum to afford $CELA_1D$-OH as a waxy yellow solid. The same procedure was followed to prepare compound $CELA_3D$-OH.

$CELA_1D$-OH. Yield: 96% (0.23 g). ^{1}H NMR (DMSO-*d*, 400 MHz): δ = 0.89 (t, 3H), 1.23−1.54 (m, 10H), 1.80 (m, 2H), 3.45 (m, 4H), 3.65 (t, 4H), 3.71 (m, 4H) 3.77 (m, 4H), 4.08 (t, 2H), 4.11 (m, 4H), 4.18 (m, 4H), 4.33 (s, 1H), 4.41 (s, 1H), 4.47 (s, 1H), 4.51 (d, 2H), 4.79 (s, 3H), 5.08 (s, 1H), 5.31 (s, 1H), 5.57 (d, 1H), 6.99 (d, 2H), 7.02 (q, 4H), 7.78 (q, 4H), 7.81 (d, 2H), 8.09 (s, 1H), 8.78 ppm (s, 1H). MS (MALDI-ToF) *m*/*z* calcd: 983.07 $[M + Na]^+$. Found: 1005.73.

$CELA_3D$-OH. Yield: 92% (0.24 g). ^{1}H NMR (DMSO-*d*, 400 MHz): δ = 0.89 (t, 9H), 1.23−1.54 (m, 30H), 1.80 (m, 6H), 3.45 (m, 4H), 3.65 (t, 12H), 3.71 (m, 4H) 3.77 (m, 12H), 4.08 (t, 6H), 4.11 (m, 4H), 4.18 (m, 12H), 4.33 (s, 1H), 4.41 (s, 1H), 4.47 (s, 1H), 4.51 (d, 2H), 4.79 (s, 3H), 5.08 (s, 1H), 5.31 (s, 1H), 5.57 (d, 1H), 7.02 (q, 12H), 7.21 (s, 2H), 7.84 (q, 12H), 8.09 (s, 1H), 8.78 ppm (s, 1H). MS (MALDI-ToF) *m*/*z* calcd: 1896.22 $[M + Na]^+$. Found: 1918.74.

Characterization Technique. ^{1}H NMR spectra were recorded on a JNM-EX400 spectrometer in deuterated chloroform ($CDCl_3$) and dimethyl sulfoxide (DMSO-*d*) at room temperature. Chemical shifts were quoted in parts per million (ppm) and referenced to tetramethylsilane (TMS). MALDI-ToF MS (Voyager-DE STR Biospectrometry Workstation) experiments were conducted to confirm the purity of the final product. UV−vis absorption spectra were obtained with a SCINCO S-3100 spectrophotometer. The change of optical textures at a given temperature was monitored by using cross-polarized POM (Nikon ECLIPSE E600POL) coupled with a heating stage (LINKAM LTS 350). An AFM (Digital Instrument, Nanoscope IIIa) technique was employed to investigate the topology of $CELA_n$D-OH surfactant monolayer film. Here, the contact mode was applied to get the height images. The force used by the cantilever was light enough to prevent the unexpected damage, but sufficient to accurately explore the surface features. The scanning rate was manipulated to be 1.0 Hz. The data were collected with the 512 × 512 pixels per image resolution. Additionally, the Cerius^2 simulation software from Accelrys (version 4.6) was also used to calculate the minimal-energy geometry in the isolated gas-phase utilizing the COMPASS force field.

■ ASSOCIATED CONTENT

Ⓢ Supporting Information

^{1}H NMR, MALDI-ToF MS and detailed experimental procedures. This material is available free of charge via the Internet at http://pubs.acs.org.

■ AUTHOR INFORMATION

Corresponding Author

*K.-U. Jeong. E-mail: kujeong@jbnu.ac.kr.

Notes

The authors declare no competing financial interest.

■ ACKNOWLEDGMENTS

This work was mainly supported by Basic Science Research (2013R1A1A2007238), KIST institutional program (2Z04320) and BK21 Plus program, Korea. D.-Y. Kim appreciates the support from Global Ph.D. Fellowship Program.

■ REFERENCES

(1) Kelker, H.; Knoll, P. M. Some Pictures of the History of Liquid Crystals. *Liq. Cryst.* **1989**, *5*, 19−42.

(2) Jeong, K.-U.; Jing, A. J.; Mansdorf, B.; Graham, M. J.; Yang, D.-K.; Harris, F. W.; Cheng, S. Z. D. Biaxial Molecular Arrangement of Rod-Disc Molecule under an Electric Field. *Chem. Mater.* **2007**, *19*, 2921−2923.

(3) Kim, J.; Khan, M.; Park, S.-Y. Glucose Sensor Using Liquid-Crystal Droplets Made by Microfluidics. *ACS Appl. Mater. Interfaces* **2013**, *5*, 13135−13139.

(4) Iglesias, W.; Abbott, N. L.; Mann, E. K.; Jákli, A. Improving Liquid-Crystal-based Biosensing in Aqueous Phases. *ACS Appl. Mater. Interfaces* **2012**, *4*, 6884−6890.

(5) Goodby, J. W.; Waugh, M. A.; Stein, S. M.; Chin, E.; Pindak, R.; Patel, J. S. Characterization of a New Helical Smectic Liquid Crystal. *Nature* **1989**, *337*, 449−452.

(6) Kikuchi, H.; Yokota, M.; Hisakado, Y.; Yang, H.; Kajiyama, T. Polymer-Stabilized Liquid Crystal Blue Phases. *Nat. Mater.* **2002**, *1*, 64−68.

(7) Shi, Y.; Fang, G.; Glaser, M. A.; Maclennan, J. E.; Korblova, E.; Walba, D. M.; Clark, N. A. Phase Winding of a Nematic Liquid Crystal by Dynamic Localized Reorientation of an Azo-based Self-Assembled Monolayer. *Langmuir* **2014**, *30*, 9560−9566.

(8) Yu, H.; Kobayashi, T. Fabrication of Stable Nanocylinder Arrays in Highly Birefringent Films of an Amphiphilic Liquid-Crystalline Diblock Copolymer. *ACS Appl. Mater. Interfaces* **2009**, *1*, 2755−2762.

(9) Takatoh, K.; Hasegawa, M.; Koden, M.; Itoh, N.; Hasegawa, R.; Sakamoto, M. *Alignment Technologies and Applications of Liquid Crystal Devices*; Taylor & Francis Inc.: New York, 2005.

DOI: 10.1021/acsami.5b00259
ACS Appl. Mater. Interfaces 2015, 7, 6195−6204

(10) Rasing, T.; Musevic, I. *Surfaces and Interfaces of Liquid Crystals*; Springer: New York, 2004.
(11) Hoogboon, J.; Garcia, P. M. L.; Otten, M. B. J.; Elemans, J. A. A. W.; Sly, J.; Lazarenko, S. V.; Rasing, T.; Rowan, A. E.; Nolte, R. J. M. Tunable Command Layer for Liquid Crystal Alignment. *J. Am. Chem. Soc.* **2005**, *127*, 11047−11052.
(12) Gin, D. L.; Lu, X.; Nemade, P. R.; Pecinovsky, C. S.; Xu, Y.; Zhou, M. Recent Advances in the Design of Polymerizable Lyotropic Liquid-Crystal Assemblies for Heterogeneous Catalysis and Selective Separations. *Adv. Funct. Mater.* **2006**, *16*, 865−878.
(13) Lu, R.; Wu, S.-T.; Lee, S. H. Reducing the Color Shift of a Multidomain Vertical Alignment Liquid Crystal Display Using Dual Threshold Voltages. *Appl. Phys. Lett.* **2008**, *92*, 0511141−0511143.
(14) Zhou, J.; Collard, D. M.; Park, J. O.; Srinivasaro, M. Control of the Anchoring Behavior of Polymer-Dispersed Liquid Crystals: Effect of Branching in the Side Chains of Polyacrylates. *J. Am. Chem. Soc.* **2002**, *124*, 9980−9981.
(15) Lee, S. H.; Lee, S. L.; Kim, H. Y. Electro-optic Characteristics and Switching Principle of a Nematic Liquid Crystal Cell Controlled by Fringe-Field Switching. *Appl. Phys. Lett.* **1998**, *73*, 2881−2883.
(16) Bisoyi, H. K.; Kumar, S. Liquid-Crystal Nanoscience: An Emerging Avenue of Soft Self-Assembly. *Chem. Soc. Rev.* **2011**, *40*, 306−319.
(17) Park, H.-G.; Lee, J.-J.; Dong, K.-Y.; Oh, B.-Y.; Kim, Y.-H.; Jeong, H.-Y.; Ju, B.-K.; Seo, D.-S. Homeotropic alignment of Liquid Crystals on a Nano-patterned Polyimide Surface Using Nanoimprint Lithography. *Soft Matter* **2011**, *7*, 5610−5614.
(18) Wang, X.; Wang, H.; Luo, L.; Huang, J.; Gao, J.; Liu, X. Dependence of Pretilt Angle on Orientation and Conformation of Side Chain with Different Chemical Structure in Polyimide Film Surface. *RSC Adv.* **2012**, *2*, 9463−9472.
(19) Glushchenko, A.; Kresse, H.; Reshetnyak, V.; Qeznikov, Y. U.; Yaroshshuk, O. Memory Effect in Filled Nematic Liquid Crystals. *Liq. Cryst.* **1997**, *23*, 241−246.
(20) Shiraishi, Y.; Toshima, N.; Meada, K.; Yoshikawa, H.; Xu, J.; Kobayashi, S. Frequency Modulation Response of a Liquid-Crystal Electro-optic Device Doped with Nanoparticles. *Appl. Phys. Lett.* **2002**, *81*, 2845−2847.
(21) Lee, W.; Wang, C.-Y.; Shih, Y.-C. Effects of Carbon Nanosolids on the Electro-optical Properties of a Twisted Nematic Liquid-Crystal Host. *Appl. Phys. Lett.* **2004**, *85*, 513−515.
(22) Ercole, F.; Davis, T. P.; Evans, R. A. Photo-responsive Systems and Biomaterials: Photochromic Polymers, Light-Triggered Self-Assembly, Surface Modification, Fluorescence Modulation and Beyond. *Polym. Chem.* **2010**, *1*, 37−54.
(23) Yager, K. G.; Barrett, C. J. Novel Photo-switching Using Azobenzene Functional Materials. *J. Photochem. Photobiol., A* **2006**, *182*, 250−261.
(24) Fang, G.; Shi, Y.; Maclennan, J. E.; Clark, N. A. Photo-reversible Liquid Crystal Alignment using Azobenzene-based Self-Assembled Monolayers: Comparison of the Bare Monolayer and Liquid Crystal Reorientation Dynamics. *Langmuir* **2010**, *26*, 17482−17488.
(25) Ichimura, K.; Suzuki, Y.; Seki, T.; Hosoki, A.; Aoki, K. Reversible Change in Alignment Mode of Nematic Liquid Crystals Regulated Photochemically by Command Surfaces Modified with an Azobenzene Monolayer. *Langmuir* **1988**, *4*, 1214−1216.
(26) Cabrera, I.; Krongauz, V.; Ringsdorf, H. Photo- and Thermochromic Liquid Crystal Polysiloxanes. *Angew. Chem., Int. Ed. Engl.* **1987**, *26*, 1178−1180.
(27) Kurihara, S.; Ikeda, T.; Tazuke, S.; Seto, J. E. Isothermal Phase Transition of Liquid Crystals Induced by Photoisomerization of Doped Spiropyrans. *J. Chem. Soc. Faraday Trans.* **1991**, *87*, 3251−3254.
(28) Krongauz, V. Photochromic Polymers. *Mol. Cryst. Liq. Cryst.* **1994**, *246*, 339−346.
(29) Dumont, M.; Osman, A. E. On Spontaneous and Photoinduced Orientational Mobility of Dye Molecules in Polymers. *Chem. Phys.* **1999**, *245*, 437−462.
(30) Ishitobi, H.; Sekkat, Z.; Kawata, S. Individualized Optically Induced Orientation of Photochemical Isomers. *Chem. Phys. Lett.* **1999**, *300*, 421−428.
(31) Chen, J.-W.; Huang, C.-C.; Chao, C.-Y. Supramolecular Liquid-Crystal Gels Formed by Polyfluorene-based π-Conjugated Polymer for Switchable Anisotropic Scattering Device. *ACS Appl. Mater. Interfaces* **2014**, *6*, 6757−6764.
(32) Kim, D.-Y.; Nayek, P.; Kim, S.; Ha, K. S.; Jo, M. H.; Hsu, C.-H.; Cao, Y.; Cheng, S. Z. D.; Lee, S. H.; Jeong, K.-U. Suppressed Crystallization of Rod-Disc Molecule by Surface Anchoring Confinement. *Cryst. Growth Des.* **2013**, *13*, 1309−1315.
(33) Park, S.-K.; Kim, S.-E.; Kim, D.-Y.; Kang, S.-W.; Shin, S.; Kuo, S.-W.; Hwang, S.-H.; Lee, S. H.; Lee, M.-H.; Jeong, K.-U. Polymer-Stabilized Chromonic Liquid-Crystalline Polarizer. *Adv. Funct. Mater.* **2011**, *21*, 2129−2139.
(34) Ichimura, K. Photoalignment of Liquid-Crystal Systems. *Chem. Rev.* **2000**, *100*, 1847−1873.
(35) Kawanishi, Y.; Tamaki, T.; Sakuragi, M.; Seki, T.; Suzuki, Y.; Ichimura, K. Photochemical Induction and Modulation of Nematic Homogeneous Alignment by the Polarization Photochromism of Surface Azobenzenes. *Langmuir* **1992**, *8*, 2601−2604.
(36) Aoki, K.; Seki, T.; Sakuragi, M.; Ichimura, K. Reversible Alignment Change of Liquid Crystals Induced by Photochromic Molecular Films. 15. Convenient Methods to Prepare "Command Surfaces" by Surface-Selective Modification of Thin Films of Poly(vinyl alcohol) with Azobenzene Units. *Makromol. Chem.* **1992**, *193*, 2163−2174.
(37) Ichimura, K.; Suzuki, Y.; Seki, T.; Kawanishi, Y.; Aoki, K. Reversible Alignment Change of Liquid Crystals Induced by Photochromic Molecular Films. 2. Reversible Alignment Change of a Nematic Liquid Crystal Induced by Pendant Azobenzene Group-Containing Polymer Thin Films. *Makromol. Chem. Rapid Commun.* **1989**, *10*, 5−8.
(38) Kim, D.-Y.; Lee, S.-A; Choi, Y.-J.; Hwang, S.-H.; Kuo, S.-W.; Nah, C.; Lee, M.-H.; Jeong, K.-U. Thermal- and Photo-induced Phase-Transition Behaviors of the Tapered Dendritic Liquid Crystal with Photochromic Azobenzene Mesogens and a Bicyclic Chiral Center. *Chem.—Eur. J.* **2014**, *20*, 5689−5695.
(39) Liu, D.; Broer, D. J. Liquid Crystal Polymer Networks: Preparation, Properties, and Applications of Films with Patterned Molecular Alignment. *Langmuir* **2014**, *30*, 13499−13509.
(40) Prompinit, P.; Achlkumar, A. S.; Bramble, J. P.; Bushby, R. J.; Wälti, C.; Evans, S. D. Controlling Liquid Crystal Alignment Using Photocleavable Cyanobiphenyl Self-Assembled Monolayers. *ACS Appl. Mater. Interfaces* **2010**, *2*, 3686−3692.
(41) Soberats, B.; Uchida, E.; Yoshio, M.; Kagimoto, J.; Ohno, H.; Kato, T. Macroscopic Photocontrol of Ion-Transporting Pathways of a Nanostructured Imidazolium-based Photoresponsive Liquid Crystal. *J. Am. Chem. Soc.* **2014**, *136*, 9552−9555.
(42) Park, C.; Lee, J.; Kim, C. Functional Supramolecular Assemblies Derived from Dendritic Building Blocks. *Chem. Commun.* **2011**, *47*, 12042−12056.
(43) Wie, J. J.; Lee, K. M.; Smith, M. L.; Vaia, R. A.; White, T. J. Torsional Mechanical Responses in Azobenzene Functionalized Liquid Crystalline Polymer Networks. *Soft Matter* **2013**, *9*, 9303−9310.
(44) Kosa, T.; Sukhomlinova, L.; Su, L.; Taheri, B.; White, T. J.; Bunning, T. J. Light-Induced Liquid Crystallinity. *Nature* **2012**, *485*, 347−349.
(45) Tanaka, D.; Ishiguro, H.; Shimizu, Y.; Uchida, K. Thermal and Photoinduced Liquid Crystalline Phase Transitions with a Rod-Disc Alternative Change in the Molecular Shape. *J. Mater. Chem.* **2012**, *22*, 25065−25071.
(46) Wu, M.-J.; Chu, C.-C.; Cheng, M.-C.; Hsiao, V. K. S. Reversible Phase Transition and Rapid Switching of Azobenzene-Doped Cholesteric Liquid Crystals with a Single Laser. *Mol. Cryst. Liq. Cryst.* **2012**, *557*, 176−189.
(47) Wang, G.; Zhang, T.; Guan, J.; Yang, H. Photoresponsive Behaviors of Smectic Liquid Crystals Tuned by an Azobenzene Chromophore. *RSC Adv.* **2012**, *2*, 487−493.

DOI: 10.1021/acsami.5b00259
ACS Appl. Mater. Interfaces 2015, 7, 6195−6204

(48) Zhang, W.; Ang, W. T.; Xue, C.-Y.; Yang, K.-L. Minimizing Nonspecific Protein Adsorption in Liquid Crystal Immunoassays by Using Surfactants. *ACS Appl. Mater. Interfaces* **2011**, *3*, 3496−3500.
(49) Dong, Y. D.; Larson, I.; Barnes, T. J.; Prestidge, C. A.; Boyd, B. J. Adsorption of Nonlamellar Nanostructured Liquid-Crystalline Particles to Biorelevant Surfaces for Improved Delivery of Bioactive Compounds. *ACS Appl. Mater. Interfaces* **2011**, *3*, 1771−1780.
(50) Malone, S. M.; Schwartz, D. K. Polar and Azimuthal Alignment of a Nematic Liquid Crystal by Alkylsilane Self-Assembled Monolayers: Effects of Chain-Length and Mechanical Rubbing. *Langmuir* **2008**, *24*, 9790−9794.
(51) Jeong, J.; Han, G.; Johnson, A. T. C.; Collings, P. J.; Lubensky, T. C.; Yodh, A. G. Homeotropic Alignment of Lyotropic Chromonic Liquid Crystals Using Noncovalent Interactions. *Langmuir* **2014**, *30*, 2914−2920.
(52) Hara, M.; Nagano, S.; Seki, T. $\pi-\pi$ Interaction-Induced Vertical Alignment of Silica Mesochannels Templated by a Discotic Lyotropic Liquid Crystal. *J. Am. Chem. Soc.* **2010**, *132*, 13654−13656.
(53) Hwang, B. H.; Ahn, H. J.; Rho, S. J.; Chae, S. S.; Baik, H. K. Vertical Alignment of Liquid Crystals with Negative Dielectric Anisotropy on an Inorganic Thin Film with a Hydrophilic Surface. *Langmuir* **2009**, *25*, 8306−8312.
(54) Weiss, K.; Woll, C.; Bohm, E.; Fiebranz, B.; Forstmann, F.; Peng, B.; Scheumann, V.; Johannsmann, D. Molecular Orientation at Rubbed Polyimide Surfaces Determined with X-ray Absorption Spectroscopy: Relevance for Liquid Crystal Alignment. *Macromolecules* **1998**, *31*, 1930−1936.
(55) Kim, N.; Kim, D.-Y.; Park, M.; Choi, Y.-J.; Kim, S.; Lee, S. H.; Jeong, K.-U. Asymmetric Organic−Inorganic Hybrid Giant Molecule: Hierarchical Smectic Phase Induced from POSS Nanoparticles by Addition of Nematic Liquid Crystals. *J. Phys. Chem. C* **2015**, *119*, 766−774.
(56) Noonan, P. S.; Shavit, A.; Acharya, B. R.; Schwartz, D. K. Mixed Alkylsilane Functionalized Surfaces for Simultaneous Wetting and Homeotropic Anchoring of Liquid Crystals. *ACS Appl. Mater. Interfaces* **2011**, *3*, 4374−4380.
(57) Qi, H.; Hegmann, T. Multiple Alignment Modes for Nematic Liquid Crystals Doped with Alkylthiol-Capped Gold Nanoparticles. *ACS Appl. Mater. Interfaces* **2009**, *1*, 1731−1738.
(58) Kim, D.-Y.; Lee, S.-A; Park, M.; Jeong, K.-U. Dual Photo-functionalized Amphiphile for Photo-reversible Liquid Crystal Alignments. *Chem.—Eur. J.* **2015**, *21*, 545−548.
(59) Kim, D.-Y.; Kim, S.; Lee, S.-A; Choi, Y.-E.; Yoon, W.-J.; Kuo, S.-W.; Hsu, C.-H.; Hunag, M.; Lee, S. H.; Jeong, K.-U. Asymmetric Organic−Inorganic Hybrid Giant Molecule: Cyanobiphenyl Mono-substituted Polyhedral Oligomeric Silsesquioxane Nanoparticles for Vertical Alignment of Liquid Crystals. *J. Phys. Chem. C* **2014**, *118*, 6300−6306.
(60) Wang, J.-X.; Chen, Q.; Bian, N.; Yang, F.; Sun, J.; Qi, A.-D.; Yang, C.-G.; Han, B.-H. Sugar-Bearing Tetraphenylethylene: Novel Fluorescent Probe for Studies of Carbohydrate-Protein Interaction Based on Aggregation-Induced Emission. *Org. Biomol. Chem.* **2011**, *9*, 2219−2226.
(61) Clemente, M. J.; Tejedor, R. M.; Romero, P.; Fitremann, J.; Oriol, L. Maltose-based Gelators Having Azobenzene as Light-Sensitive Unit. *RSC. Adv.* **2012**, *2*, 11419−11431.
(62) Hutt, O. E.; Mulet, X.; Savage, G. P. Click-Chemistry as a Mix-and-Match Kit for Amphiphile Synthesis. *ACS Comb. Sci.* **2012**, *14*, 565−569.
(63) Györgydeák, Z.; Szilágyi, L.; Paulsen, H. Synthesis, Structure, and Reactions of Glycosyl Azides. *J. Carbohydr. Chem.* **1993**, *12*, 139−163.
(64) Choi, Y.-E.; Oh, S. H.; Jo, M. H.; Jang, I. W.; Kim, S.-E.; Jeong, K.-U.; Lee, S. H. Nano-particle Induced VA-LCD. *SID Int. Symp. Dig. Technol. Pap.* **2012**, *43*, 1415−1417.
(65) Dierking, I. *Textures of Liquid Crystals*; Wiley-VCH: Weinheim, Germany, 2003.

DOI: 10.1021/acsami.5b00259
ACS Appl. Mater. Interfaces 2015, 7, 6195−6204